

## An Effective Iris Recognition System

Hsiau Wen Lin<sup>1</sup>, Hwei Jen Lin<sup>\*2</sup>, Yue Sheng Li<sup>2</sup>

<sup>1</sup>Department of Information Management, Chihlee institute of Technology  
New Taipei City, Taiwan, R.O.C.

<sup>2</sup>Department of Computer Science and Information Engineering, Tamkang University  
New Taipei City, Taiwan, R.O.C.

\*Corresponding author, e-mail: 086204@mail.tku.edu.tw

### Abstract

An iris recognition system uses the iris to distinguish the identity of a person using the rich iris texture feature. To effectively remove noise and precisely segment the stable iris region is a crucial stage prior to recognition. Most noises on iris images are caused by occlusion of eyelids or eyelashes in certain areas. In this paper, we propose an iris recognition system which precisely locates and segments iris regions. We extract the iris feature from a relatively reliable portion of the iris region using a DoG filter. Experimental results show that the proposed iris recognition system has satisfactory results in terms of time efficiency and recognition rate.

**Keywords:** biometric recognition, iris recognition, iris segmentation, iris normalization, feature extraction.

**Copyright © 2014 Institute of Advanced Engineering and Science. All rights reserved.**

### 1. Introduction

The biometric recognition technique is a scientific solution to recognizing individuals based upon biological characteristics like appearance, iris, face, fingerprints, voice, and hand geometry [1-3]. Voice and hand geometry recognition are too unstable at their present stage of technological development. Iris recognition is the most precise of all biometric identification systems [4-10].

The iris is a circular structure with texture in the eye between the cornea and lens, controlling the size of the pupil and the light reaching the eye. In 1987, Leonard Flom and Aran Safir [1] conducted clinical experiments which showed that irides will no longer change from birth to one year to one and a half year later. According to statistics, the probability of two irides having the same features is about  $1/10^{78}$ . Moreover, iris texture is not hereditary; even for twins, their irides are not the same. In addition, an iris is extremely difficult to copy because it is located inside the eye and the size is changed by light. Therefore, an iris offers uniqueness and stability for recognition.

The first automatic iris recognition system was developed by Daugman [4-6]. This system used an integrodifferential operator (IDO) to detect the inner and outer boundaries of the iris. In the normalization step, the iris region is resampled to a rectangular image to compensate for the various sizes of different eye images. Finally, a 2D Gabor filter was used for feature extraction. Mehrotra proposed sector-based normalization [11] to eliminate the range most likely to be occluded by eyelashes and eyelids.

Iris detection is a crucial stage for a successful iris recognition system [11-17]. In this study we propose a method of iris feature extraction, which consists of four modules: segmentation, normalization, noise removal, and feature extraction. This method precisely locates a stable iris region to extract reliable iris features for recognition. Before extraction of iris features, it is essential to remove the noise, such as in the eyelids and eyelashes region, since the noise factors taken as a part of the iris texture will seriously diminish the recognition accuracy rate. This study focuses on locating the iris region and selects only non-occluded regions to extract features, in hopes of improving recognition performance.

The rest of the paper is organized as follows: Section 2 describes the proposed iris recognition method. Some experimental results and comparison with other methods are described in Section 3, and the last section provides our conclusions.

## 2. Iris Recognition System

The proposed iris recognition system includes the following steps: inner boundary detection, outer boundary detection, iris normalization, feature extraction and feature matching. Each of the steps is described below.

### 2.1. Inner Boundary Detection

The inner boundary is located between the pupil and iris. Chou [10] used connected component analysis and an ellipse fitting algorithm to find the pupil. However, ellipse fitting is time consuming and not suitable for eye images with too much eyelashes-covered area. We improve the pupil detection method proposed by Chou. First, a threshold value  $T$  for image binarization is determined by (1), where  $\mu_s$  is the lowest intensity value and  $\mu_w$  is the average intensity of the image.

$$T = \frac{\mu_s + \mu_w}{2} \quad (1)$$

And then, connected component analysis is used to discard the regions which are either too large or too small. From the remaining regions, the one closest to the image center is selected as the pupil candidate, as shown in Figure 1.

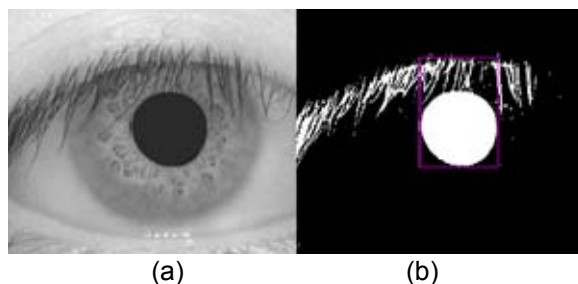


Figure 1. (a) eye image, (b) rectangular region on the binarized eye image obtained by connected component analysis.

In order to remove noise caused by eyelashes, morphological opening (erosion followed by dilation) is performed. A result of this operation is shown in Figure 2.

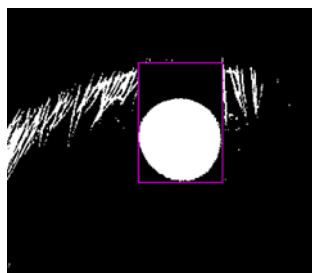


Figure 2. Result of Opening Operation

In some binarized eye images, holes might be caused by camera reflection, as shown in Figure 3. To fill up the holes, morphological closing (a dilation followed by an erosion) is performed, as shown in Figure 4.

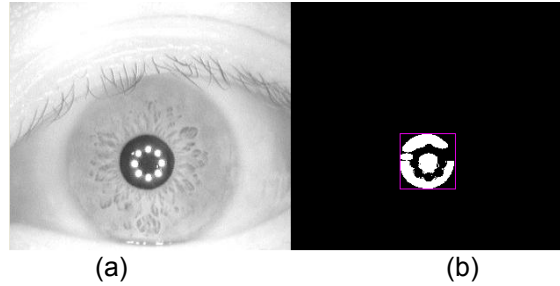


Figure 3. (a) Eye Image with Reflection, (b) Result after Opening with holes in the pupil area.

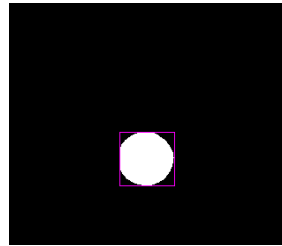


Figure 4. Result of Closing Operation

However, in some cases, the rectangle includes part of the eyelid, as shown in Figure 5. To refine the rectangle, we use the horizontal projection and vertical projection of the enclosed image as shown in Figure 6(a), and find the positions with projection values smaller than a given threshold to form the boundaries of a new rectangle, as shown in Figure 6(b).

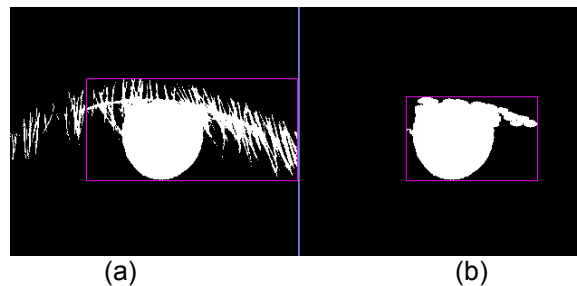


Figure 5. (a) Pupil Image Connected with Eyelid, (b) Result of Morphological Process

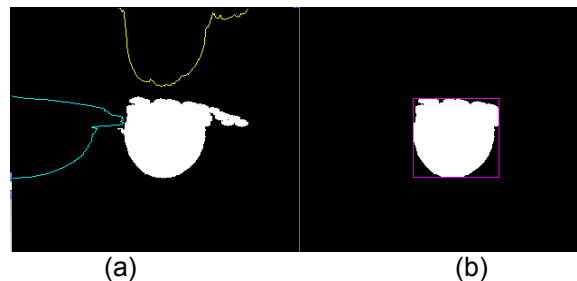


Figure 6. (a) Horizontal Projection and Vertical Projection, (b) A More Suitable Enclosing Rectangle Obtained using Projection Results

## 2.2. Outer Boundary Detection

The outer boundary is located between the sclera and iris. In most cases, the center of the iris inner boundary is close to the center of the iris outer boundary. We design two masks to

detect the leftmost position and the rightmost position, respectively, of the outer boundary, as shown in Figure 7. Each of the two masks is applied on a specific rectangular region of the image. The center of the rectangle for detecting the leftmost position and the center of the detected pupil boundary are of the same height. Moreover, the distances from the left bound of pupil to the right bound and the left bound of the rectangle are denoted by  $min$  and  $max$ , respectively. The values of  $min$  and  $max$  can be used represent a lower bound and an upper bound for the radii difference between pupil and iris. The height of the rectangle is taken as the lower  $2/3$  of the height of the detected pupil boundary, as shown in Figure 8. Consider the rectangle for detecting the leftmost position of the outer boundary, in which each pixel is convolved with the mask shown in Figure 7(a). Rows of convolved values in the rectangle are then summed up, and the location with the maximum accumulating value is regarded as the leftmost position of the outer boundary. The rightmost position of the outer boundary of the iris can be determined in the same manner.



Figure 7. Masks for Detecting (a) Leftmost Position and (b) Rightmost Position of the Outer Boundary

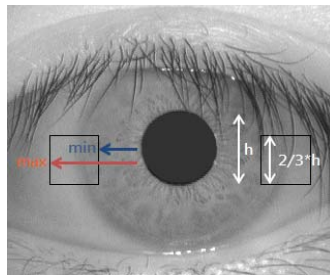


Figure 8. Filter Processing Range

With both the leftmost position and the rightmost position of the outer boundary, the diameter can be determined by drawing a horizontal line segment, through the center of the pupil, from the leftmost position to the rightmost position, and consequently, the outer boundary is formed, as shown in Figure 9.

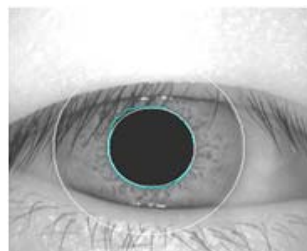


Figure 9. Iris Segmentation Result

### 2.3 Iris Normalization

After obtaining the iris region  $I(x, y)$ , we normalize it by translating it from an  $xy$ -coordinate system into a polar coordinate system using the rubber-sheet method [4-6], as represented by (2), where  $\gamma$  and  $\theta$  denote the radial coordinate and the angular coordinate, respectively, with  $0 \leq \gamma \leq 64$  and  $0 \leq \theta < 360$ .

$$I(x(\gamma, \theta), y(\gamma, \theta)) \rightarrow I(\gamma, \theta) \tag{2}$$

That is, for pixel  $(\gamma, \theta)$  in the new plane, its value is the value of pixel  $(x(\gamma, \theta), y(\gamma, \theta))$  in the raw plane, where  $x(\gamma, \theta)$  and  $y(\gamma, \theta)$  can be determined by (3) and (4), where  $(x_i, y_i)$  and  $(x_o, y_o)$  are the points lying on the inner boundary and outer boundary, respectively, as shown in Figure 10. An example of the mapping is shown in Figure 11.

$$x(\gamma, \theta) = \frac{64 - \gamma}{64} x_i(\theta) + \frac{\gamma}{64} x_o(\theta) \tag{3}$$

$$y(\gamma, \theta) = \frac{64 - \gamma}{64} y_i(\theta) + \frac{\gamma}{64} y_o(\theta) \tag{4}$$

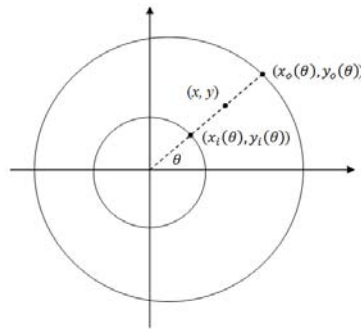


Figure 10. Rubber-sheet Method

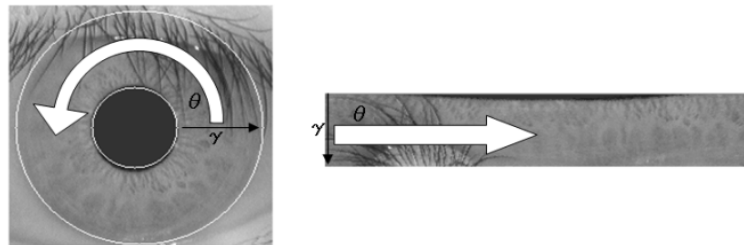


Figure 11. Rubber-sheet Method (a) Detected Iris Region, (b) the Transform Region (360\*64)

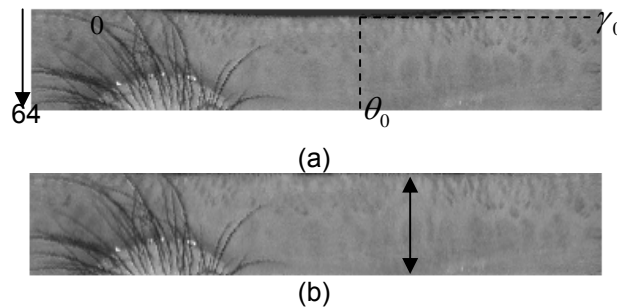


Figure 12. Removing Pupil by Linear Interpolation

However, the iris region determined in the above manner is very likely to include part of the pupil, since the pupil is not a perfect circle, as shown in Figure 11(a). As shown in Figure

11(b), in the portion of the pupil distributed along the upper part of the rectangle after normalization, the boundary between pupil and iris in the rectangle can be detected using an edge detection method, and then the portion of the pupil can be removed by performing linear interpolation on the radial of the rectangle along the angular coordinate axis. As shown in Figure 12(a), in column  $\theta_0$  of the rectangle, the detected pupil boundary is at  $\gamma = \gamma_0$ , and so the lower part of length  $64 - \gamma_0$  is occupied by the iris, which is then scaled by factor  $64/(64 - \gamma_0)$  to fill up the whole column. The portion of the pupil in the rectangle can be removed by removing the portion of pupil in each column in this manner, and at the same time, the resulting rectangle is further normalized.

Mehrotra [11] proposed sector-based normalization to exclude some unreliable regions, which are frequently occluded by the eyelids and eyelashes. However, many unreliable regions still remain, as shown in Figure 13.

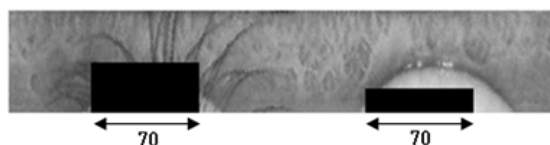


Figure 13. Regions Removed by Sector-based Normalization [11]

To raise the recognition rate, we remove more unreliable regions,  $35 \leq \theta \leq 146$ ,  $225 \leq \theta \leq 316$ , and  $61 \leq \gamma \leq 64$ , as shown in Figure 14. Finally, the remaining regions are merged into a smaller rectangle, as shown in Figure 15.

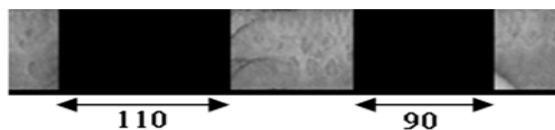


Figure 14. Regions Removed by Our Method

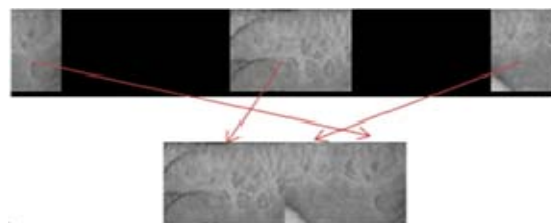


Figure 15. Normalized Iris Image

#### 2.4. Feature Extraction

To enhance the contrast of iris texture caused by weak illumination, histogram equalization is performed on the normalized image, as shown in Figure 16.



Figure 16. Result of Histogram Equalization on Figure 15

Finally, we extract the iris feature from the image obtained after performing histogram equalization by convolving it with the Difference of Gaussian (DoG) as defined in (5), where  $(u, v)$  determines the position of the filter center,  $\sigma$  is the standard derivation and  $K$  is the ratio of two standard derivation used in each Gaussian blur. The iris code is set to 1 when the convolved value is larger than zero, and otherwise set to 0. The feature code of the image given in Figure 10 is shown in Figure 17.

$$f(u, v, \sigma) = \frac{1}{2\pi\sigma^2} \exp^{-\frac{(u^2+v^2)}{(2\sigma^2)}} - \frac{1}{2\pi K^2\sigma^2} \exp^{-\frac{(u^2+v^2)}{(2K^2\sigma^2)}} \quad (5)$$



Figure 17. Feature Extraction Result

### 2.5. Feature Matching

The features of the test image are compared with the feature of each image in the database using Hamming distance, as shown in (6), where the  $A$  and  $B$  are two compared iris codes,  $N$  is the size of each iris code, and  $\oplus$  denotes the exclusive OR operator.

$$HD = \frac{1}{N} \sum_{i=1}^N (A_i \oplus B_i) \quad (6)$$

### 3. Experimental Results

In this section, we will evaluate our proposed method for iris recognition on two data sets, CAISA V1.0 and CAISA V3.0, from the public database CASIA [18], where CAISA V1.0 contains 756 iris images from 108 different eyes (i.e., 108 classes) and CAISA V3.0 contains 2639 iris images from 395 different eyes (i.e., 395 classes). All images in both datasets are 320x240 in size in grayscale. In CAISA V1.0, each class has 7 images. 90 classes were regarded as legal users and the rest as impostors, the first 6 images from each legal class were taken as training samples and the last one was kept for testing. In CAISA V3.0, each class has 1 to 26 images. We regard the 286 classes with more than 5 images as legal users and the rest as impostors, and train the system by using the first 5 images. The performance indices are chosen as equal error rate (EER), where the false accept rate (FAR) and the false reject rate (FRR) are equal.

In the first experiment, we attempt to verify whether the reliable portion we chose is more effective than that chosen by Mehrotra [11] or the whole iris region.

Table 1. Results of Our Method Based on Different Iris Region Portions Testing on CASIA V1.0.

	Whole region	Portion chosen by Mehrotra	Portion chosen by our method
EER(%)	3.81	2.35	0
FRR(FAR=0%)	6.66	3.33	0

Table 2. Comparison of Our Method with the Method Proposed by Mehrotra Tested on CASIA V3.0

	Mehrotra	Our method
FAR(%)	4.58	3.39
FRR(%)	3.85	3.9
EER(%)	4.23	3.73

In the second experiment, we compare the performance of our method with the method proposed by Mehrotra [11], where the result of Mehrotra's method tested on CAISA V3.0 was taken from [11], as shown in Table 2.

#### 4. Conclusion

In this paper, we proposed an iris recognition system which precisely locates and segments iris regions. We extract iris features from a more reliable portion of the iris region using the DoG filter. Experimental results show that the feature extracted from the remaining reliable portion is still able to distinguish the identity of a person. Moreover, it not only saves time for detecting eyelashes and eyelids, but also improves the recognition rate.

In our future work, we will take into account more non-ideal images, such as iris images with in-plane rotation or non-orthogonal view iris images.

#### References

- [1] L Flom, A Safir. Iris recognition system. U. S. Patent no. 4641349, 1987.
- [2] Patricia Melin, Víctor Herrera, Danniela Romero, Fevrier Valdez, Oscar Castillo, Genetic Optimization of Neural Networks for Person Recognition based on the Iris. *TELKOMNIKA Indonesian Journal of Electrical Engineering*. 2012; 10(2): 309–320.
- [3] Jianbo Yao, Tao Zhang. Biometric Cryptosystem Based Energy Attack Analysis. *TELKOMNIKA Indonesian Journal of Electrical Engineering*. 2012; 10(5): 1130–1136.
- [4] J Daugman. High confidence visual recognition of persons by a test of statistical independence. *IEEE Trans. on Pattern Analysis and Machine Intelligence*. 1993; 15: 1148-1161.
- [5] J Daugman. How iris recognition works. *IEEE Trans. on Circuits and Systems for Video Technology*. 2004; 14: 21-30
- [6] J Daugman. New methods in iris recognition. *IEEE Trans. on Systems, Man, and Cybernetics, Part B: Cybernetics*. 2007; 37: 1167-1175.
- [7] RP Wildes, JC Asmuth, GL Green, SC Hsu, RJ Kolczynski, JR Matey, SE McBride. *A system for automated iris recognition*. Proceedings of the Second IEEE Workshop on Applications of Computer Vision. 1994; 121-128.
- [8] RP Wildes. *Iris recognition: an emerging biometric technology*. Proceedings of the IEEE. 1997; 85: 1348-1363.
- [9] DRS Kumar, KB Raja, N Nuthan, B Sindhuja, P Supriya, RK Chhotaray, S Pattnaik. *Iris recognition based on DWT and PCA*. Proceedings of 2011 International Conference on Computational Intelligence and Communication Networks (CICN). 2011; 489-493.
- [10] Chia-Te Chou, Sheng-Wen Shih, Wen-Shiung Chen, Victor W. Cheng, Duan-Yu Chen. Non-orthogonal view iris recognition system. *IEEE Trans. Circuits and Systems for Video Technology*. 2010; 20: 417-430.
- [11] H Mehrotra, GS Badrinath, B Majhi, P Gupta. *An efficient iris recognition using local feature descriptor*. Proceedings of 2009 16th IEEE International Conference on Image Processing (ICIP). 2009; 1957-1960.
- [12] Zhaofeng He, Tieniu Tan, Zhenan Sun, Xianchao Qiu. *Robust eyelid, eyelash and shadow localization for iris recognition*. Proceedings of 15th IEEE International Conference on Image Processing. 2008; 265-268.
- [13] Tae-Hong Min, Rae-Hong Park. *Comparison of eyelid and eyelash detection algorithms for performance improvement of iris recognition*. Proceedings of 15th IEEE International Conference on Image Processing. 2008; 257-260.
- [14] Namrata P Joshi, Roopal K Lamba, Devang U Shah, Bhargav V Ghadia. *Implementation of various approaches for iris image normalization*. Proceedings of 2011 Nirma University International Conference on IEEE Engineering (NUICONE). 2011; 1-5.
- [15] Byung Jun Kang, Kang Ryoung Park. A robust eyelash detection based on iris focus assessment. *Pattern Recognition Letters*. 2007; 28: 1630-1639.
- [16] R Chen, XR Lin, TH Ding. Iris segmentation for non-cooperative recognition system. *Image Processing, IET*. 2011; 5: 448-456.
- [17] DM Monro, S Rakshit, D Zhang. DCT-based iris recognition. *IEEE Trans. on Pattern Analysis and Machine Intelligence*. 2007; 29: 586-596.
- [18] Chinese Academy of Sciences Institute of Automation. CASIA V1.0 Iris Image Database. <http://biometrics.idealtest.org/>